Visualizing buried silicon atoms at the Cd-Si(111)-7 × 7 interface with localized electrons

Min-Long Tao,[1] Hua-Fang Xiao,[1] Kai Sun,[1] Yu-Bing Tu,[1] Hong-Kuan Yuan,[1] Zu-Hong Xiong,[1] Jun-Zhong Wang,[1,*] and Qi-Kun Xue[2,†]

[1]*School of Physical Science and Technology, MOE Key Laboratory on Luminescence and Real-Time Analysis, Southwest University, Chongqing 400715, China*

[2]*State Key Laboratory of Low-Dimensional Quantum Physics, Department of Physics, Tsinghua University, Beijing 100084, China*

(Received 11 May 2017; revised manuscript received 27 July 2017; published 7 September 2017; corrected 11 September 2017)

We report the atomic-scale imaging of the buried Cd-Si(111)-7 × 7 interface with a low temperature scanning tunneling microscopy (STM). The Cd(0001) films grown on Si(111)-7 × 7 reveal the electronic growth mode, and manifest a series of quantum-well states. In the low-bias STM images, not only the 7 × 7 reconstruction but also individual Si adatoms buried by thick Cd islands are clearly visible. The two successive layers of Cd islands exhibit the distinct contrasts due to the quantum size effect. Moreover, we found a small gap appeared at Fermi level owing to the Anderson localization induced by interface scattering. The perfect transparency of Cd films can be attributed to the anisotropic electron motion, i.e., lateral electron localization and transverse motion like free-electron.

DOI: 10.1103/PhysRevB.96.125410

Interfacial structures play a crucial role in determining the morphology of epitaxial thin films. Studying the interfacial structures and their evolution is essential to our understanding of growth mechanism of epitaxial films. In the past decades, significant progress has been made in probing the interface structure of epitaxial films with various experimental techniques [1,2]. However, it remains a big challenge to visualize the interface structure nondestructively at the atomic scale. It is well known that scanning tunneling microscopy (STM) is a powerful tool to resolve the surfaces structures and electronic states at atomic scale [3,4]. As an extension, it would be intriguing to apply this method to detect the buried interface structure.

Recently, it has been demonstrated that STM is capable of revealing the structures of buried metal-semiconductor interfaces [5–15]. Altfeder *et al.* used the quantized electrons in quantum well state (QWS) to image the step edges of a Si(111) substrate underlying Pb islands [5]. The Pb islands seem to be transparent because the interface structure of Pb-Si(111) can also be directly imaged [6–8]. However, Si adatoms were not resolved, only 7 × 7 reconstruction was observed. Such transparency of the Pb islands was caused by strong electronic anisotropy associated with the electron localization [8,16–20]. Beside the interface structures, subsurface objects such as the nanocavities in metals [21–25], the dopants in semiconductor can be also detected by means of scanning tunneling spectra (STS) due to the formation of QWSs [26–28].

Compared with the fcc metal Pb, the divalent hexagonal close packed (hcp) metal Cd are less reminiscent of a free-electron metal because of the strong repulsive interaction between the 4*d* state and the conduction bands [29–31]. It manifests some anisotropic behaviors in thermal conductivity, electron mean free path, and superconducting gaps [32–34]. Moreover, relativistic effects may be important for Cd due to the considerable spin-orbit coupling.

In this paper we demonstrate that the Cd(0001) films grown on Si(111)-7 × 7 surface exhibit a perfect transparency. Not only the buried Si(111)-7 × 7 lattices but also the individual Si adatoms can be clearly resolved in the low-bias STM images. Compared with the partial preservation of the Si(111)-7 × 7 surface and the alloying of Pb and Si, the Cd-covered Si(111)-7 × 7 surface remains intact without any alloying, indicating a weak Cd-Si interaction. A small gap associated with the bound state has been found near Fermi level, indicating that the Anderson localization induced by interface scattering is responsible for the perfect transparency of Cd(0001) films.

The experiments were conducted in a Unisoku low-temperature STM system with a base pressure of 1.2×10^{-10} mbar. A clean Si(111)-7 × 7 surface was used as substrate for Cd deposition. The Si(111)-7 × 7 surface was prepared by repeated flashing to ∼1100 °C after overnight degassing. High purity (99.998%) Cd was deposited from a BN cell by sublimating to ∼430 K, while the Si(111) sample was kept at room temperature. The deposition rate is around ∼0.35 ML/ min (here we define the amount of Cd atoms in the wetting layer as two monolayers). A W tip was used for all the STM measurement at ∼78 K, while a polycrystalline Pt-Ir tip was used for all the STS investigation at ∼78 or 4.2 K. All differential conductance dI/dV spectra were acquired using a standard lock-in technique with a bias modulation of 10 mV at 1999 Hz.

Figure 1(a) shows the morphology of Cd films formed on Si(111)-7 × 7 at low coverage (4.0 ML). Flattop Cd islands with elongated geometry prefer to attach the step edges of Si(111), indicating the anisotropic diffusion of Cd atoms resulted from the Ehrlich-Schwoebel barrier. Among the individual Cd islands, there are disordered wetting layers [Fig. 1(b)]. Careful analysis shows that the island heights in Fig. 1(a) are confined at 5.8, 17.0, and 20.5 Å above the wetting layer, respectively, corresponding to 2, 6, and 7 ML of Cd(0001) films [35]. Particularly, the 7 ML is the most abundant. Here we determine the thickness of the Cd island by measuring the height from wetting layer to the island top, then convert it into the layer number along the [0001]

*jzwangcn@swu.edu.cn
†qkxue@mail.tsinghua.edu.cn

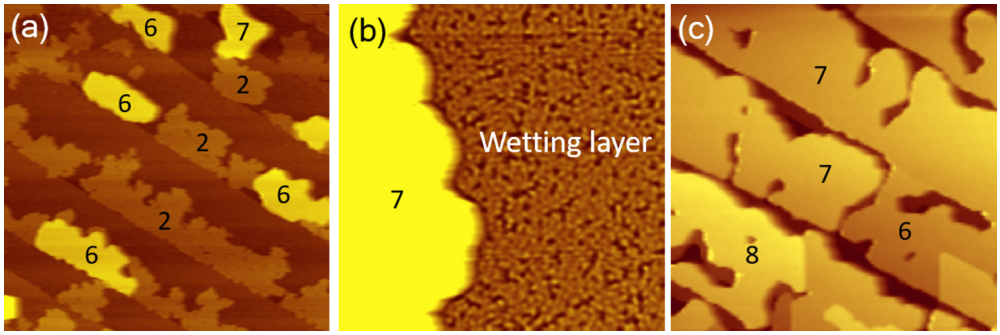

FIG. 1. Morphology of the Cd(0001) films grown on Si(111)-7 × 7 surface. The black numbers represent a discrete height of 2, 6, 7, and 8 ML on top of the wetting layer. (a) and (b) Isolated Cd islands formed at low coverage. (a) 1000 × 1000 nm^2, 3.0 V, (b) 100 × 100 nm^2, 2.4 V. (c) Coalescence of the Cd islands within a single Si terrace at high coverage, 550 × 550 nm^2, 3.0 V. There is no mass transportation across the Si step due to the large Ehrlich-Schwoebel barrier.

direction of the cadmium crystal (the interlayer spacing is 2.8 Å). With coverage increasing, the islands prefer to grow in size instead of in height. The Cd islands start to coalesce within a single terrace when the coverage reaches 7.0 ML as shown in Fig. 1(c). When the coverage increases further, both the lateral growth and on-top growth proceed simultaneously. However, we cannot find the Cd islands with the thickness 3, 4, and 5 ML from our extensive experiments. The critical and magic thicknesses found here imply that the growth process is similar to the reported "electronic growth" mode in the films of Pb on Si(111) [8,36,37] and Ag on GaAs(110) [38]. The physical origin can be attributed to the interplay between the effects of quantum confinement, charge spilling, and interface-induced Friedel oscillations [38].

To our surprise, the topographic STM images of Cd islands can provide the structural information of buried Cd-Si(111) interface. Figure 2(a) shows the low-bias STM image of a 14 ML Cd island, where the underlying Si(111)-7 × 7 lattices at the interface are clearly visible. Not only the faulted and unfaulted half-unit cells, but also the six Si adatoms can be clearly discerned. The corresponding fast Fourier transform (FFT) image is displayed at the top of Fig. 2(b), where the 7 × 7 vectors and $2a_0$ spacing of Si adatom are consistent with the pristine Si(111)-7 × 7 surface. Such perfect transparency of Cd islands reveals a higher lateral resolution of the interface structures than the Pb-Si and In-Si system, because the latter lacks the resolved image of Si adatoms. From the zoom-in image in Fig. 2(c), it is found that the 7 × 7 lattices and Si adatoms remain intact. There is a fuzzy protrusion inside the corner hole of Si(111)-7 × 7 surface, which might be the filled Cd adatoms or the modification of electronic states of the pristine Si(111)-7 × 7 surface due to the charge transfer. Such complete conservation of Si(111)-7 × 7 surface demonstrates that the Cd-Si interaction is weaker than Pb-Si. When the bias increased to 0.2 V, the corner holes and dimer rows become vague, but the Si adatoms can be still resolved [Fig. 2(d)]. Further increasing of bias to 0.7 V, the resolution of interface structure reduces significantly [Fig. 2(e)]. Only the two half-unit cells of the 7 × 7 reconstruction can be resolved, resembling the STM image of Pb islands on Si(111) [6]. We noticed that the STM imaging of buried interface is influenced by the QWSs confined in the Cd islands. When the bias voltage is coincident with the peak position in the dI/dV spectra (QWSs), the atomic-scale image of the buried Si(111)-7 × 7 interface can be obtained. However, when the bias voltage is far away from the peaks and close to the valley position in the dI/dV spectra, the buried Si(111)-7 × 7 interface is difficult to be imaged with atomic resolution. In this situation, the top surface of Cd(0001) islands can be imaged with atomic resolution. The hexagonal lattices [Fig. 2(f)] reveal a lattice constant of 3.0 Å, close to that of a crystalline Cd(0001) plane.

In addition, we noticed some bright protrusions distributed randomly at the Cd-Si(111) interface. We speculated that they are small Cd clusters originated from the Cd wetting layer. Upon the Cd island formation, the disordered wetting layer beneath the Cd islands essentially transformed into crystalline hcp structure, leaving a small part of Cd atoms remaining in the disordered arrangement. In other words, the Cd islands contact directly with the underlying Si substrate, instead of on top of the wetting layer, consistent with the Pb islands [39]. In the case of Pb or In on Si(111), there were similar bright protrusions, which were supposed to be Pb-Si alloy [6,8]. It means that some Si adatoms of Si(111) have been removed from their initial positions and the Si(111)-7 × 7 surface has been modified to some extent.

Due to the misfit of step height between Si (3.13 Å) and Cd (2.80 Å) a mesalike Cd island across a Si step may be formed (Fig. 3). The mesa surface reveals a slight height difference (∼0.5 Å) between the left part (6 ML) and the right part (7 ML). At 1.0 V, the 6 ML Cd reveals a higher resolution than the 7 ML Cd. When the bias is reduced to 0.6 V, the situation is reversed in that the 7 ML Cd exhibits a higher resolution than the 6 ML Cd. Such contrast of N and $N + 1$ layers in Cd islands can be attributed to the different distribution of electronic density of state (DOS).

Beside the lateral resolution of Cd islands, the apparent height of Cd clusters also reveals a complementary behavior between the two successive Cd layers. Figure 4 shows a mesalike Cd island divided by a diagonal step of Si(111). The upper left part is 7 ML Cd, while the lower right part is 8 ML Cd. In the filled-state STM image (−1.0 V), the apparent height of Cd clusters is 20 pm in the 7 ML Cd, while it is 50 pm in the 8 ML. As a result, the 7 ML Cd looks smoother than the 8 ML Cd. In the empty-state image (0.8 V), the situation

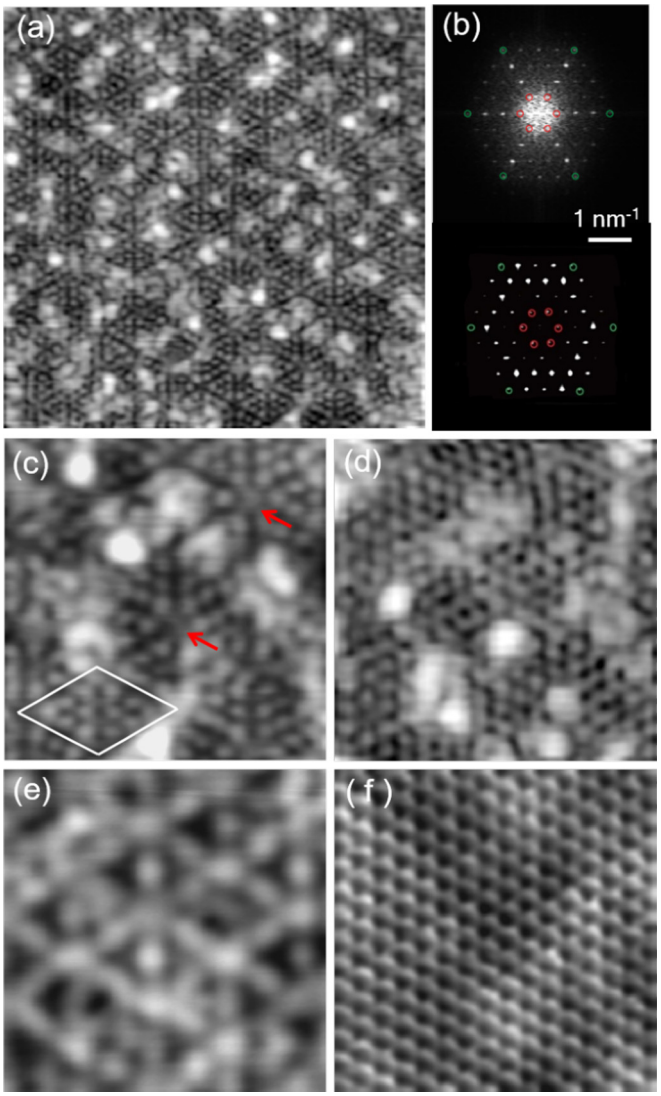

FIG. 2. The perfect transparency of Cd(0001) film on Si(111)-7 × 7. (a) Large-scale STM image acquired on top of a 14 ML Cd island, 0.1 V, 30 × 30 nm^2. (b) Fast Fourier transform (FFT) of (a) (up) and Si(111)-7 × 7 (down). The red spots correspond to the 7 × 7 lattices, the green spots to the spacing between Si adatoms. (c)–(e) Close-up views of the Cd-Si(111) interface recorded at 0.1, 0.2, and 0.7 V, respectively, 10 × 10 nm^2. The red arrows mark the positions of corner hole of Si(111)- 7 × 7. (f) Atomically revolved STM image of top surface of Cd island, 4 × 4 nm^2, 0.6 V.

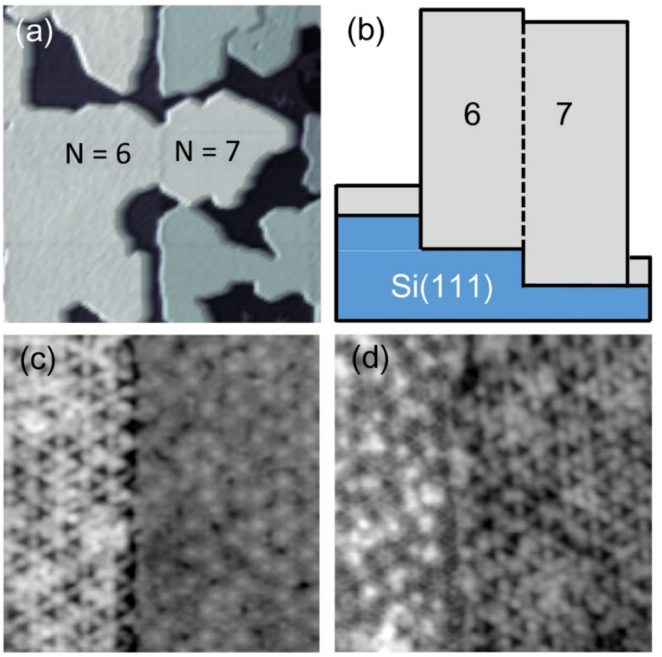

FIG. 3. Complementary contrasts between the two successive layers Cd islands. (a) A mesalike Cd island crossing a Si(111) step with 6 ML thickness at the right side and 7 ML thickness at the left side, 480 × 480 nm^2, 3.0 V. (b) A sketch to illustrate the structure of mesalike Cd island in (a). Due to the misfit of step height between Si and Cd, a slight height difference (∼0.5 Å) appeared at the Si step. (c) and (d) The close-up views of the mesa recorded at 1.0 and 0.6 V, respectively. The vertical boundary is originated from the underlying atomic step of the Si substrate, 30 × 30 nm^2.

is reversed in that the 8 ML Cd looks smoother than the 7 ML Cd.

In Fig. 5(a) we show a series of the dI/dV spectra acquired on the Cd islands with different thickness. The spectra exhibit a number of peaks associated with the QWSs due to the vertical electron confinement in a one-dimensional quantum box. With increasing island thickness, the energy separation between the peaks decreases and more peaks appear. We summarized the spectra data in Fig. 5(b), where the energies of QWSs versus Cd island height are plotted. It is found that the middle position between the highest occupied subbands (HOS) and the lowest unoccupied subbands (LUS) oscillates with the film thickness with a periodicity of 5 ML, distinct from the bilayer oscillation periodicity in Pb islands [36]. Based on the standing wave condition, the electron oscillation periodicity should correspond to the half wavelength: $\lambda_F/2 \approx 5a$. The thickness variation of Cd for one layer would bring a spectra shift $\delta \approx \Delta(2a/\lambda_F)$ [5,8]. As shown in Fig. 5(c), we find the spectra shift $\delta \approx \Delta/5$ for the Cd island on Si(111), indicating $\lambda_F \approx 10a$. It is consistent with the observation in Fig. 5(b). In Fig. 5(d) we plot the inverse of an energy separation as a function of island thickness H. The data can be fitted by $\Delta = \pi\hbar v_F/H$, $\hbar$ is the Planck's constant and v_F is the Fermi velocity. A Fermi velocity $v_F = 2.2 \times 10^8$ cm/s can be obtained by fitting from 6 to 20 ML. It is close to the reported value 1.6×10^8 cm/s in bulk Cd metal [40]. The negative thickness offset implies that the disordered Cd wetting layer becomes ordered upon further deposition of Cd atoms, and the Cd islands contact with the underlying Si substrate directly as mentioned above.

According to the theoretical calculation of the electronic structures of metal Cd, the energy band along the ΓA direction is steeper than along the ΓM and ΓK directions [30–32]. The ratio of the effective masses of electrons normal and parallel to the Cd(0001) films, $\alpha = m^*_\perp/m^*_\parallel$, is estimated to be 1/6, indicating the electrons have the anisotropic motions in Cd. Meanwhile, based on the reported measurements using magnetoacoustic oscillation or de Haas–van Alphen effect, no parallel segment can be identified from the Fermi surface sections of Cd crystal along ΓA (transversal

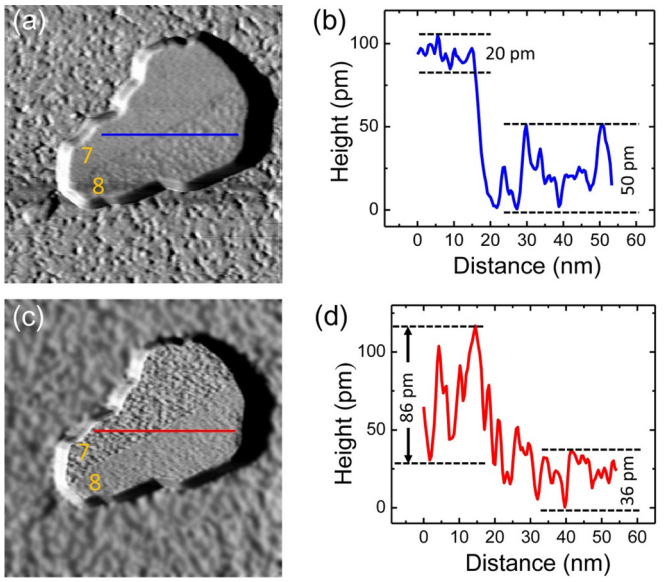

FIG. 4. The Cd clusters located at the interface reveal a complementary transparent height between the two successive layers islands. (a) Filled-state STM image of a mesalike island, −1.0 V, $110 \times 110\,\mathrm{nm}^2$. The diagonal boundary divides the Cd island into two parts. The lower right part (8 ML) looks "rougher" than the upper left part (7 ML). (b) Cross-sectional line profile taken along the blue line in (a). (c) Empty-state STM image of the same mesalike islands as (a), 0.8 V, $110 \times 110\,\mathrm{nm}^2$. The lower right part (8 ML) looks "smoother" than the upper left part (7 ML). (d) Cross-sectional line profile taken along the red line in (c).

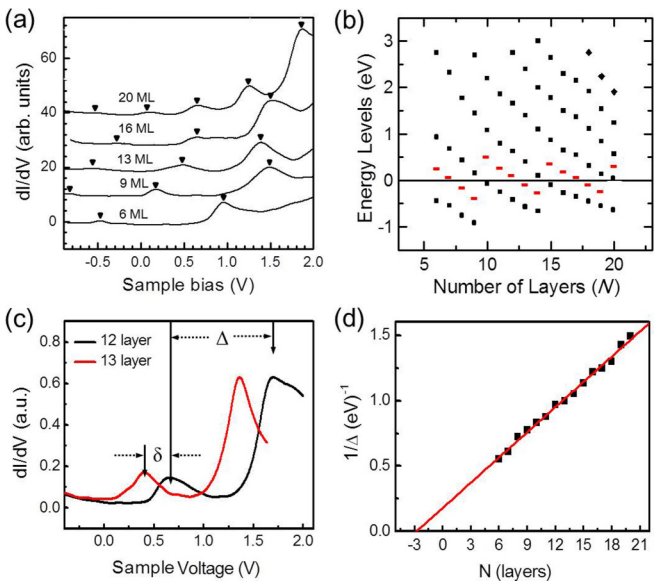

FIG. 5. (a) A series of dI/dV spectra acquired on the Cd islands of varying thickness, $U = 1.5\,\mathrm{V}$, $I = 1\,\mathrm{nA}$. The numbers indicate the thickness of Cd islands above wetting layer. Triangles show the extracted QWS energy. Spectra are vertically shifted for clarity. (b) The energies of quantum-well state versus Cd island height. The short red bars mark the middle position between the highest occupied subbands (HOS) and the lowest unoccupied subbands (LUS). (c) Spectra shift brought by introducing 1 ML Cd on top the 12 ML Cd island. (d) The inverse of energy separation between the subbands as a function of island thickness. The red solid line is a fit to the data with $v_F = 2.2 \times 10^8\,\mathrm{cm/s}$.

direction) and ΓM or ΓK (lateral directions). These previous experiments reveal the bulk cadmium does not have a nested Fermi surface [40–42]. Thus, the perfect transparency cannot be mainly attributed to the electronic structure of metal Cd.

In order to elucidate the enhanced lateral resolution, we measured the dI/dV spectra close to Fermi level at different sites of the Cd island surface [Fig. 6(a)]. It is found that all the sites of Cd island surface show a small gap around 10 meV. Particularly, the spectra acquired atop the Cd clusters reveal a slightly larger gap (∼10.4 meV) and larger peaks, while the spectra acquired at other sites reveal a little bit smaller gap (∼9.5 meV) and very smaller peaks [Fig. 6(b)]. With the temperature increased from 4.7 to 12 K, the width and depth of zero-bias dip are reduced [Fig. 6(c)]. At first glance, this gap is similar to a BCS superconducting gap, but it still exists even at 5 T magnetic field, and the zero-bias conductance is far from zero. Thus, the small gap observed here is not related to the superconducting transition of Cd(0001) films.

In epitaxial graphene grown on Ru(0001), a similar localized state near Fermi energy has been observed. The electron localization was attributed to the periodic modulation of graphene-Ru interaction induced by Moiré pattern [43]. Meanwhile, Anderson localization caused by disorder or electron scattering may lead to the metal-insulator transition or formation of bound states. As a result, the local density of state (LDOS) spectra will reveal a gap at Fermi energy, which manifest itself as a cusplike dip at $V = 0$ in the scanning tunneling spectra due to the depletion of the LDOS. Here we attributed the small gap in Fig. 6(b) to the Anderson localization induced by interface scattering, same as the metal-insulator transition [44]. The gap decreases as the temperature increases because the Anderson localization is suppressed by thermal fluctuation. The perfect transparency of Cd(0001) films can be interpreted in terms the interface scattering occurred at the periodic boundary of Si(111)-7 × 7 and at the disordered Cd clusters. The buried dimer rows and corner holes of the Si(111)-7 × 7 serve as subsurface scatter centers for the lateral localization, playing a similar role as the Moiré pattern in graphene. The slightly larger gap appearing on the Cd clusters demonstrates that the electrons are scattered more significantly from the Cd clusters than those from dimer rows and corner holes [Fig. 6(d)]. As a result, the electrons confined in Cd island oscillate between its opposite boundaries with a typical free electron velocity, and possess a large in-plane effective mass. Unlike the Pb-Si or In-Si interface, the electronic anisotropy was ascribed to the enhanced many-body interactions facilitated by the transverse confinement in Pb or In films.

The buried Cd-Si(111)-7 × 7 interface has been imaged at atomic scale with a LT-STM. Beside the 7 × 7 reconstruction, the individual Si adatoms underlying the thick Cd islands can be clearly resolved. A series of QWSs have been detected in the two-dimensional Cd islands with varying heights. Moreover, a small gap (∼10 mV) near Fermi level has been observed with larger peaks acquired on top of Cd clusters, indicating the Anderson localization induced by interface scattering. The

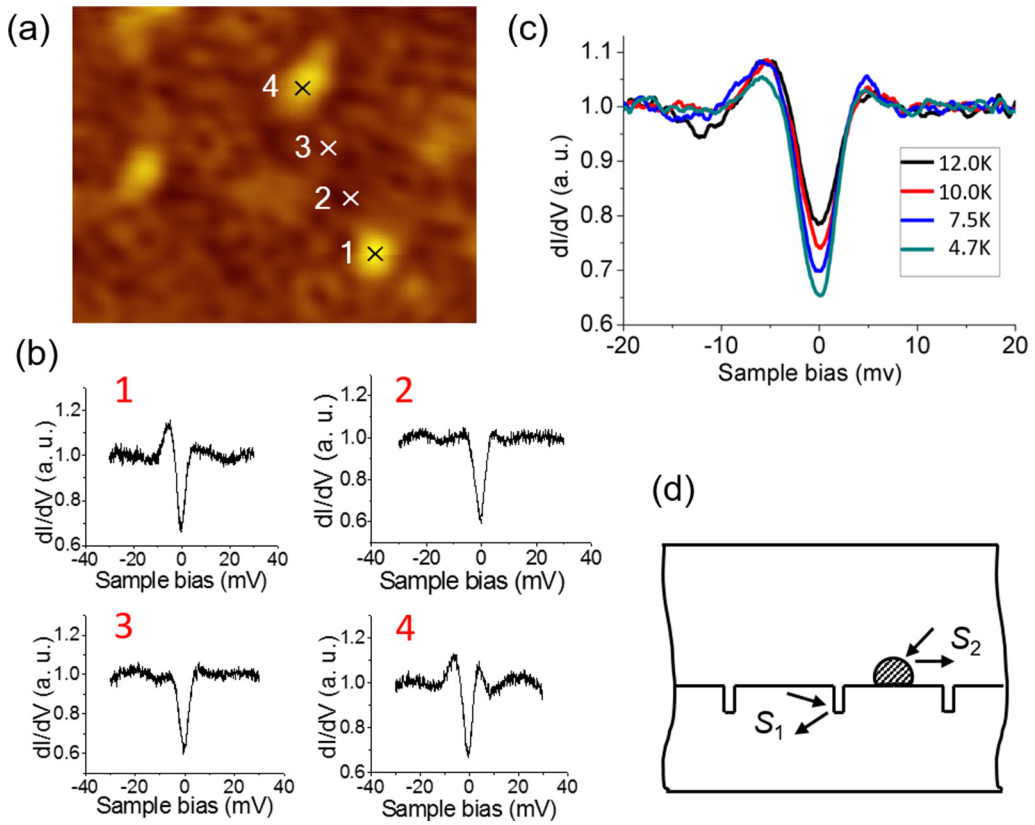

FIG. 6. (a) STM image of the 8 ML Cd island, $10 \times 10\,\mathrm{nm}^2$, 1.0 V. (b) dI/dV spectra closed to Fermi energy taken at the marked positions in (a), 1.0 V, 100 pA. The spectra taken on top of the Cd clusters (labeled with 1 and 4) show more evident peaks than the other sites (labeled with 2 and 3). (c) dI/dV spectra obtained at various temperatures, 1.0 V, 100 pA. (d) Schematic illustration of the two types of interface scattering occurred at Cd-Si(111). The S_1 type scattering occurred at the periodic corner holes of Si(111)-7 × 7, corresponding to the nonadiabatic interface. The S_2 type scattering occurred at the disordered Cd clusters.

perfect transparency of Cd films can be attributed to the strong anisotropic electron motion with large lateral effective mass. We hope that our results will be helpful to understand the impacts of the lateral localization and transverse quantization on the detecting of the buried interface structure at atomic scale.

This work was supported by the National Natural Science Foundation of China (Grants No. 11574253, No. 10974156, No. 21173170, No. 91121013, and No. 11604269) and the Fundamental Research Funds for the Central Universities (XDJK2017C064, XDJK2016C065).

M.-L.T and H.-F.X. contributed equally to this paper.

[1] F. Hoehne, J. M. Lu, A. R. Stegner, M. Stutzmann, M. S. Brandt, M. Rohrmuller, W. G. Schmidt, and U. Gerstmann, Phys. Rev. Lett. **106**, 196101 (2011).

[2] J. D. Emery, B. Detlefs, H. J. Karmel, L. O. Nyakiti, D. K. Gaskill, M. C. Hersam, J. Zegenhagen, and M. J. Bedzyk, Phys. Rev. Lett. **111**, 215501 (2013).

[3] M. F. Crommie, C. P. Lutz, and D. M. Eigler, Nature (London) **363**, 524 (1993).

[4] Y. Hasegawa and P. Avouris, Phys. Rev. Lett. **71**, 1071 (1993).

[5] I. B. Altfeder, K. A. Matveev, and D. M. Chen, Phys. Rev. Lett. **78**, 2815 (1997).

[6] I. B. Altfeder, D. M. Chen, and K. A. Matveev, Phys. Rev. Lett. **80**, 4895 (1998).

[7] I. B. Altfeder, V. Narayanamurti, and D. M. Chen, Phys. Rev. Lett. **88**, 206801 (2002).

[8] I. B. Altfeder, X. Liang, T. Yamada, D. M. Chen, and V. Narayanamurti, Phys. Rev. Lett. **92**, 226404 (2004).

[9] I. Altfeder, K. A. Matveev, and A. A. Voevodin, Phys. Rev. Lett. **109**, 166402 (2012).

[10] J. A. Kubby and W. J. Greene, Phys. Rev. Lett. **68**, 329 (1992).

[11] S. Heinze, R. Abt, S. Blugel, G. Gilarowski, and H. Niehus, Phys. Rev. Lett. **83**, 4808 (1999).

[12] C. Didiot, A. Vedeneev, Y. Fagot-Revurat, B. Kierren, and D. Malterre, Phys. Rev. B **72**, 233408 (2005).

[13] C. Rogero, J. A. Martin-Gago, and J. I. Cerda, Phys. Rev. B **74**, 121404 (2006).

[14] Y. Oh, J. Seo, H. Suh, J. S. Seo, S.-J. Kahng, and Y. Kuk, Surf. Sci. **602**, 3352 (2008).

[15] M. Yakes and M. C. Tringides, J. Phys. Chem. A **115**, 7096 (2011).

[16] J. H. Dil, J. W. Kim, T. Kampen, K. Horn, and A. R. H. F. Ettema, Phys. Rev. B **73**, 161308 (2006).
[17] Y. Liu, J. J. Paggel, M. H. Upton, T. Miller, and T. C. Chiang, Phys. Rev. B **78**, 235437 (2008).
[18] A. Mans, J. H. Dil, A. R. H. F. Ettema, and H. H. Weitering, Phys. Rev. B **66**, 195410 (2002).
[19] M. H. Upton, T. Miller, and T. C. Chiang, Phys. Rev. B **71**, 033403 (2005).
[20] B. Slomski, F. Meier, J. Osterwalder, and J. H. Dil, Phys. Rev. B **83**, 035409 (2011).
[21] M. Schmid, W. Hebenstreit, P. Varga, and S. Crampin, Phys. Rev. Lett. **76**, 2298 (1996).
[22] O. Kurnosikov, O. A. O. Adam, H. J. M. Swagten, W. J. M. de Jonge, and B. Koopmans, Phys. Rev. B **77**, 125429 (2008).
[23] O. Kurnosikov, J. H. Nietsch, M. Sicot, H. J. M. Swagten, and B. Koopmans, Phys. Rev. Lett. **102**, 066101 (2009).
[24] O. Kurnosikov, H. J. M. Swagten, and B. Koopmans, Phys. Rev. Lett. **106**, 196803 (2011).
[25] M. Müller, N. Néel, S. Crampin, and J. Kröger, Phys. Rev. Lett. **117**, 136803 (2016).
[26] M. C. M. M. van der Wielen, A. J. A. van Roij, and H. van Kempen, Phys. Rev. Lett. **76**, 1075 (1996).
[27] J. M. Jancu, J. C. Girard, M. O. Nestoklon, A. Lemaitre, F. Glas, Z. Z. Wang, and P. Voisin, Phys. Rev. Lett. **101**, 196801 (2008).
[28] K. Sinthiptharakoon, S. R. Schofield, P. Studer, V. Brazdova, C. F. Hirjibehedin, D. R. Bowler, and N. J. Curson, J. Phys.: Condens. Matter **26**, 012001 (2014).
[29] R. W. Stark and L. M. Falicov, Phys. Rev. Lett. **19**, 795 (1967).
[30] S. Daniuk, T. Jarlborg, G. Kontrymsznajd, J. Majsnerowski, and H. Stachowiak, J. Phys.: Condens. Matter **1**, 8397 (1989).
[31] H. S. Chauhan, L. Ilver, P. O. Nilsson, J. Kanski, and K. Karlsson, Phys. Rev. B **48**, 4729 (1993).
[32] R. A. Robbins and B. J. Marshall, Phys. Rev. B **13**, 4852 (1976).
[33] J. D. N. Cheeke and E. Duclasoa, J. Low Temp. Phys. **11**, 687 (1973).
[34] N. V. Zavaritskii, Sov. Phys. JETP-USSR **12**, 831 (1961).
[35] D. A. Edwards, W. E. Wallace, and R. S. Craig, J. Am. Chem. Soc. **74**, 5256 (1952).
[36] W. B. Su, S. H. Chang, W. B. Jian, C. S. Chang, L. J. Chen, and T. T. Tsong, Phys. Rev. Lett. **86**, 5116 (2001).
[37] V. Yeh, L. Berbil-Bautista, C. Z. Wang, K. M. Ho, and M. C. Tringides, Phys. Rev. Lett. **85**, 5158 (2000).
[38] Z. Zhang, Q. Niu, and C. K. Shih, Phys. Rev. Lett. **80**, 5381 (1998).
[39] R. Feng, E. H. Conrad, C. Kim, P. F. Micelli, and M. C. Tringides, Physica B **357**, 175 (2005).
[40] M. R. Daniel and L. Mackinnon, Philos. Mag. **8**, 537 (1963).
[41] D. F. Gibbons and L. M. Falicov, Philos. Mag. **8**, 177 (1963).
[42] D. C. Tsui and R. W. Stark, Phys. Rev. Lett. **16**, 19 (1966).
[43] D. Stradi, S. Barja, C. Díaz, M. Garnica, B. Borca, J. J. Hinarejos, D. Sánchez-Portal, M. Alcamí, A. Arnau, A. L. Vázquez de Parga, R. Miranda, and F. Martín, Phys. Rev. B **85**, 121404 (2012).
[44] A. K. Raychaudhuri, K. P. Rajeev, H. Srikanth, and N. Gayathri, Phys. Rev. B **51**, 7421 (1995).